Ordered Mesoporous Carbons Supported Wacker-type Catalyst for Catalytic Oxidative Carbonylation

Bing Yan, Shouying Huang, Qingsen Meng, Yongli Shen, Shengping Wang, and Xinbin Ma
Key Laboratory for Green Chemical Technology of Ministry of Education, School of Chemical Engineering and Technology, Tianjin University, Tianjin 300072, China

DOI 10.1002/aic.14091
Published online April 15, 2013 in Wiley Online Library (wileyonlinelibrary.com)

Ordered mesoporous carbons (OMCs) were used as supports to prepare Wacker-type catalysts for diethyl carbonate (DEC) synthesis by oxidative carbonylation of ethanol in a gas-phase reaction. The effect of support structure on the dispersion of the active species and catalytic properties were investigated. Nitrogen sorption, X-ray diffraction (XRD) and transmission electron microscopy (TEM) results revealed that the active components have encapsulated in pore channels of OMCs. Characterizations of the catalysts, such as TEM, scanning electron microscope (SEM) and XRD, indicated that active components supported on OMCs have better dispersion compared to activated carbon (AC). The ethanol conversion of the catalysts was improved by ~65% using OMCs as the catalyst support than AC. The stability of the catalytic activity can also be enhanced through surface modification of OMCs. Surface oxygen-containing groups (OCGs) on OMCs before and after surface modification were characterized by transmission IR spectra and the Beohm titration. The relationship between surface OCGs and anchor ability of OMCs was studied. © 2013 American Institute of Chemical Engineers *AIChE J*, 59: 3797–3805, 2013
Keywords: oxidative carbonylation, OMCs, dispersion, OCGs, diethyl carbonate, ethanol

Introduction

Diethyl carbonate (DEC) has attracted much attention as a widely used building block due to its excellent biodegradability (e.g., low bioaccumulation and persistence) and low toxicity. The potential industrial applications of DEC cover many fields, such as nonpoisonous solvent, alternative substitute for phosgene, fuel additive and intermediate for the synthesis of polycarbonates and polyurethanes.[1–6] Among several methods for DEC synthesis, vapor phase oxidative carbonylation of ethanol is in line with the principles of green chemistry and represents one of the proposed favorable processes.[4–12] The reaction can be expressed as follows

$$2C_2H_5OH + CO + 1/2O_2 \rightarrow C_2H_5OCOOC_2H_5 + H_2O \quad (1)$$

Wacker-type catalysts, containing $CuCl_2$ in combination with $PdCl_2$ and other additives, e.g., KCl and NaOH, have been widely studied due to its good catalytic performance in DEC synthesis by the oxidative carbonylation.[8,10,12–16] The influence of different carriers, such as silica, alumina and activated carbon (AC), on catalytic activities was studied.[8] The catalysts which used silica as support produced considerable byproducts, and, thus, possessed poor selectivity. Copper species on alumina were more selective for DEC than the silica-supported catalysts, but the inclusion of palladium (II) chloride greatly diminished the yield of DEC. Among these supports, AC has exhibited optimum catalytic activity, with good ethanol conversion and DEC selectivity.[8] However, the microporous dominating structure of AC has restricted the dispersion of active components supported which is related to the catalytic activity.[15] Indeed, the support plays an important role in the dispersion state of active components on catalysts, and it has been widely accepted that high-surface area and large-pore volume are beneficial for the dispersion of active components.[17,18] As one of the most promising materials, ordered mesoporous carbons (OMCs) have attracted numerous attention for applications in electrode materials, energy storage and catalysis.[19–23] OMCs possess several unique properties, including high-specific surface area, large-pore volumes, uniform and tunable pore sizes, high thermal and mechanical stability, and chemical inertness.[23–26] These excellent textural characteristics enable OMCs to function as promising candidates for applications as catalyst supports.

In this study, OMCs were used as supporting materials of Wacker-type catalysts for DEC synthesis by the gas phase oxidative carbonylation of ethanol. TEM, SEM and XRD were used to assess dispersion states of active components of the catalysts. To rationalize the good catalytic properties of catalysts using OMCs as the support, catalysts loaded on AC were also synthesized for comparison. Additionally, to stabilize catalyst activity, OMCs were modified by HNO_3 and the oxygen-containing groups (OCGs) on the surface of OMCs were studied by transmission IR spectra and the Beohm titration. The relationship between surface properties of the support and catalytic stability was studied.

Correspondence concerning this article should be addressed to X. Ma at xbma@tju.edu.cn.

Experimental

Chemicals

Pluronic P123 ($EO_{20}PO_{70}EO_{20}$, $M_{av} = 5800$ g mol^{-1}) was acquired from Sigma-Alorich. Other reagents, including $CuCl_2 \cdot 2H_2O$ (AR, the third chemical reagent plant in Tianjin), $PdCl_2$ (AR, Shanghai MingHao Metal Material Co., Ltd.), activated carbon (AC) (KunShan Actview Carbon Technology Co., Ltd.), tetraethyl orthosilicate (TEOS), sucrose, NaOH, Na_2CO_3, $NaHCO_3$, concentrated sulfuric acid, hydrochloric acid, and nitric acid, methanol, ethanol (AR, Tianjin Kermel Chemical Co., Ltd.), were used without further purification unless specifically mentioned.

Catalyst preparation

OMCs were synthesized via the nanocasting route using mesoporous silica SBA-15 as an exotemplate and sucrose as the carbon source according to protocols in the literature.[26] For preparation of SBA-15, P123 and TEOS were used as a template and a silica source, respectively.[27,28] Carbonization proceeded at 1173 K in N_2 for 6 h and SBA-15 was dissolved in a 1M NaOH solution (50% H_2O, 50% ethanol). Before the impregnation of the active component, the OMCs were treated with 1M HCl at 333 K for 2 h to neutralize the surface alkalinity formed in the template removing process. The resultant sample upon filtered was washed to the neutral pH and dried at 393 K for 4 h.

A solution was prepared by dissolving $CuCl_2$, $PdCl_2$ and KCl in 100 mL methanol at 333 K. Pretreated OMCs were added to the solution and the resultant mixture was stirred vigorously at 333 K for 6 h. Subsequently, the methanol was evaporated away under the reduced pressure. The residual mixture was dried at 353 K for 4 h in a vacuum oven. In this process, the atomic ratio of Cu/Pd maintained 20 and molar ratio of KCl/Cu kept 1. The mixture was again impregnated in a sodium hydroxide methanol solution (Cu/OH = 1, molar ratio), and treated by the same procedure described earlier.[8,12] Catalysts made by this technique were denoted as $nCuCl_2$-$PdCl_2$-KCl-NaOH/OMC (nCPKN/OMC). Herein "n" represents the contents of loading species expressed by weight percentage of copper. Contents of palladium, potassium and sodium were defined through calculation in proportion mentioned previously.

Catalysts which used AC as the support were prepared by the same method and were denoted as $nCuCl_2$-$PdCl_2$-KCl-NaOH/AC (nCPKN/AC).

The treated process with HNO_3 detailed as follows. OMCs (1 g) were added to 100 mL nitric acid solution and then heated at 333 K for 2 h. The concentration of nitric acid was regulated from 5M to 9M. The obtained sample was washed to neutral, dried at 393 K for 4 h and recorded as OMC-mHNO_3 (m represents the concentration of HNO_3 treating OMCs). Then the sample was impregnated with $CuCl_2$, $PdCl_2$, KCl and NaOH by the same method mentioned previously. This kind of catalyst was marked as $nCuCl_2$-$PdCl_2$-KCl-NaOH/OMC-mHNO_3 (nCPKN/OMC-mHNO_3). The catalyst used for comparison in this part was also prepared. In order to eliminate the influence of chlorine, OMCs were used directly without being treated by HCl. However, the catalyst obtained by this method was denoted as $nCuCl_2$-$PdCl_2$-KCl-NaOH/OMC* (nCPKN/OMC*).

Characterization

Pore distribution and specific surface area of the samples were determined by nitrogen adsorption-desorption measurements performed at the 77 K on a Micromeritics Tristar 3000 analyzer. Before the analysis, the samples were degassed at 573 K for 4 h *in vacuo*. The specific surface areas were calculated from the isotherms using the BET method, and the cumulative volumes of pores were obtained by the BJH method from the desorption branches of the adsorption isotherms.

XRD measurements were performed using a Rigaku C/max-2500 diffractometer employing the graphite filtered Cu Kα radiation ($\lambda = 1.5406$ Å) at 40 kV. Diffraction data were collected using a scanning rate of 0.02°/step in a 2θ range from 0.5 to 5° with a scanning time of 1.2 s/step at 100 mA and from 10 to 90° with a scanning time of 0.3 s/step at 200 mA.

Transmission electron microscopy (TEM) images were recorded on a Philips TECNAI G^2F20 system equipped with energy dispersion X-ray spectroscopy (EDX). The samples for TEM and EDX were prepared by placing a few drops of sample suspension in ethanol onto a Ni grid followed by slow evaporation of solvent at ambient condition.

Surface morphology and composition of catalysts was examined by a Hitachi S4800 field scanning electron microscopy (SEM) equipped with an energy dispersive X-ray spectrometer (EDX). The accelerating voltage of the microscope was 5.0 kV.

Transmission IR spectra were acquired using a Thermo Scientific Nicolet 6700 (32 scans, 4 cm^{-1}). To acquire infrared spectra, each carbon sample was diluted to 0.1 wt % in dry IR-quality KBr (Fisher). Pellets (1 cm dia.) were formed from 100 mg of the diluted carbon-KBr powder. Spectrum was baseline corrected in the region from 1750 cm^{-1} to 750 cm^{-1}, and these spectra were compared on a common absorbance scale to assess the type and relative abundance of oxygen groups present on the different supports.

For the Boehm titration, one gram of carbon sample was placed in 50 mL of the following solutions: sodium hydroxide, sodium carbonate and sodium bicarbonate.[29–32] The samples were dispersed by ultrasonic for 20 min, heated at 373 K for 1.5 h and then filtered. Five milliliters of the filtrate was pipetted and the excess base was titrated with HCl. The number of acidic sites was determined under the assumptions that NaOH neutralizes carboxylic, lactonic, and phenolic groups, Na_2CO_3 neutralizes carboxylic and lactonic groups, and $NaHCO_3$ neutralizes only carboxylic groups.

XPS analysis was carried out on a PerkinElmer PHI 1600 ESCA system operated at pass energy of 187.85 eV for survey spectra with an Al KR X-ray source. The acceleration voltage was 15 kV, the power was 250 W, and the analysis area was 0.8 mm^2. Possible deviations caused by electric charge on the samples were corrected through taking the C 1 s line as an internal standard at 284.6 eV. Multipak software 8.0 was used for data treatment. The element contents were calculated through peak areas by sensitivity factor correction.

For acidity evaluation, NH_3-TPD measurements were run on a Micromeritics Autochem II 2920 instrument equipped with a TCD. The sample ($\sim$100 mg) was pretreated at 393 K for 1 h in a flow of Ar followed by NH_3 adsorption at 333 K. Desorbed NH_3 was monitored at a heating rate of 10 K min^{-1} from 333 K to 1273 K.

Catalytic measurements

Catalytic performance was evaluated in a continuous microreactor system comprising a quartz tubular reactor with

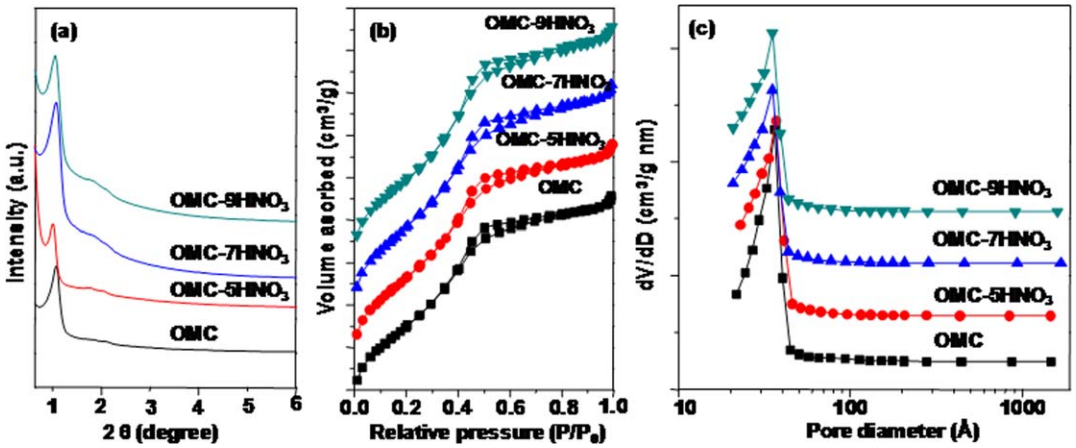

Figure 1. (a) Small-angle XRD patterns, (b) N_2 sorption isotherms, and (c) pore-size distributions of OMC and nCPKN/OMC.

[Color figure can be viewed in the online issue, which is available at wileyonlinelibrary.com.]

an inner diameter of 7 mm. The catalysts used for evaluation were pressed into 20–40 mesh. (The condition eliminating the effluence of internal diffusion) Reaction products were analyzed online by a gas chromatography (Agilent 7890GC) equipped with four columns. Two Porapak Q 80/100 and one Molesieve 13X 60/80 packed columns (Restek) connected to a TCD detector for measuring CO, O_2, and CO_2; and a DB-624 capillary column (Agilent) connected to an FID detector for measuring ethanol, DEC, and other organic byproducts. A run was initiated by loading 100 mg of catalyst diluted by quartz sands to the reactor. The reactant gases including CO (52%), O_2 (3%), ethanol (11%) and N_2 (34%) were passed over the catalyst at 90 cm^3/min (STP). (The condition eliminating the effluence of external diffusion) Reaction temperature maintained at 413 K and reaction pressure held at 0.7 MPa. The byproducts observed including acetal and acetaldehyde, and the selectivity of DEC was determined by Eq. 2

$$S_{DEC} = \frac{2[CH_3CH_2OCOOCH_2CH_3]}{[[CH_3CHO]+3[CH_3CH(OCH_2CH_3)_2]+2[CH_3CH_2OCOOCH_2CH_3]} \quad (2)$$

Results and Discussion

Structural properties of nCPKN/OMC catalysts

Figure 1a presents small-angle XRD patterns of catalysts with different loading in comparison with pure OMC. All samples possess a peak ~1° indexed as reflection of (100) of the 2D p6mm hexagonal mesostructure. The (100) peaks of nCPKN/OMC have a shift toward high-angle compared to that of OMC, indicating that the pore size of the catalysts reduces after loading active components. This trend became more obvious with the increasing of active component loading (Figure 1c). Figure 1b and c show the N_2-sorption isotherms and pore size distributions, which reveal that all the samples possess isotherms with well-defined H1 hysteresis loops, characteristic of mesoporous structure. Table 1 summarizes the textural parameters of these samples. When loaded by active components, the specific surface area of the catalysts has greatly reduced in sequence, from 1376 m^2/g to 657 m^2/g. The pore volume has also reduced from 1.38 cm^3/g to 0.66 cm^3/g, while the pore diameter maintained at the same level. This suggests that the active components enter into the pore channels of OMCs without blocking the pore. In order to further verify this hypothesis, TEM of OMC and catalysts has been done.

Figure 2 shows TEM images of OMC-based catalysts with different loading. Long 1-D channels along the (100) direction as well as hexagonally arranged pores along the (001) direction are observed clearly, indicating that the ordered mesoporous structure remains intact without being blocked upon loading active components. The pore sizes, measured in TEM images, are close to the values calculated by BJH method using N_2-adsorption branches. Combined with the results obtained previously, we deduce that active species are entered into the pore of OMCs and well dispersed. However, until the copper load increases to 10%, e.g., 10CPKN/OMC, some small black clusters appear on the surface. These involve the dispersion of catalysts and will be discussed in the following section.

Dispersion of nCPKN/OMC catalysts

In order to understand the elementary composition of the particles appeared on the surface of 10CPKN/OMC (Figure 2), composition of two representative areas (areas 1 and 2) was determined by EDX. Herein, area 1 is where the black particles appeared and area 2 is where without aggregated particles. The inset table in Figure 2 listed the elemental analysis for Cu, Na, K, Cl at the specified areas on 1°CPKN/OMC. The Cu content in areas 1 and 2 is at the same level.

Table 1. Textural Parameters of OMC and nCPKN/OMC

	S_{BET}(m^2/g)	V(cm^3/g)	d(Å)
OMC	1376	1.38	35
3CPKN/OMC	1243	1.27	34
5CPKN/OMC	1047	1.06	34
10CPKN/OMC	657	0.66	34

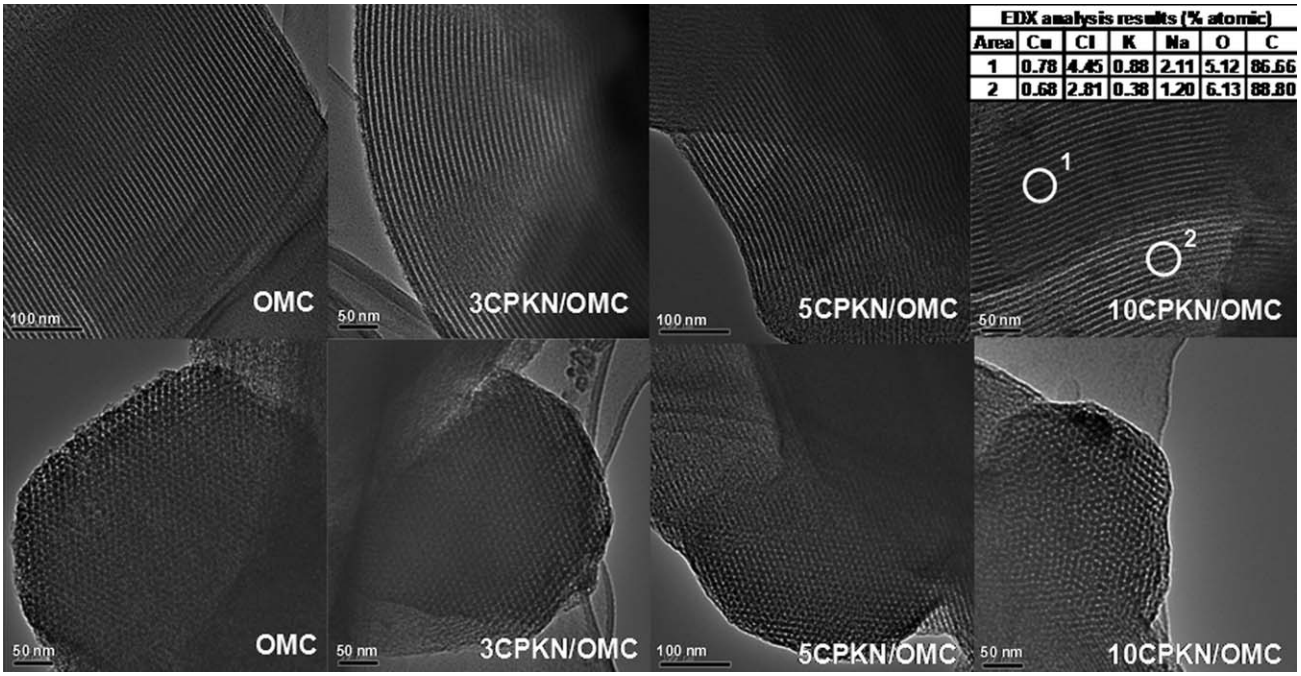

Figure 2. TEM images of OMC and nCPKN/OMC.

Values in the table are EDX results for marked areas.

Table 2. Chemical Composition of Catalysts Gained from EDX Analysis (% Atomic).

	Cu		Cl		K		Na		O		C	
Area	1	2	1	2	1	2	1	2	1	2	1	2
3CPKN/OMC	0.19	0.22	1.40	1.30	0.27	0.25	0.78	0.68	5.21	5.36	92.15	92.19
3CPKN/AC	0.21	0.17	1.50	1.43	0.34	0.27	0.81	0.79	5.16	5.28	91.98	92.06
5CPKN/OMC	0.38	0.33	2.20	2.10	0.47	0.40	1.10	0.99	5.06	5.17	90.79	91.01
5CPKN/AC	0.37	0.34	2.18	1.11	0.49	0.27	1.28	0.55	5.78	5.62	89.9	92.11
10CPKN/OMC	0.65	0.56	3.77	2.37	0.78	0.56	1.87	0.87	5.33	4.99	87.6	90.65
10CPKN/AC	0.56	0.37	3.81	1.90	0.81	0.51	1.98	0.91	5.02	4.89	87.82	91.42

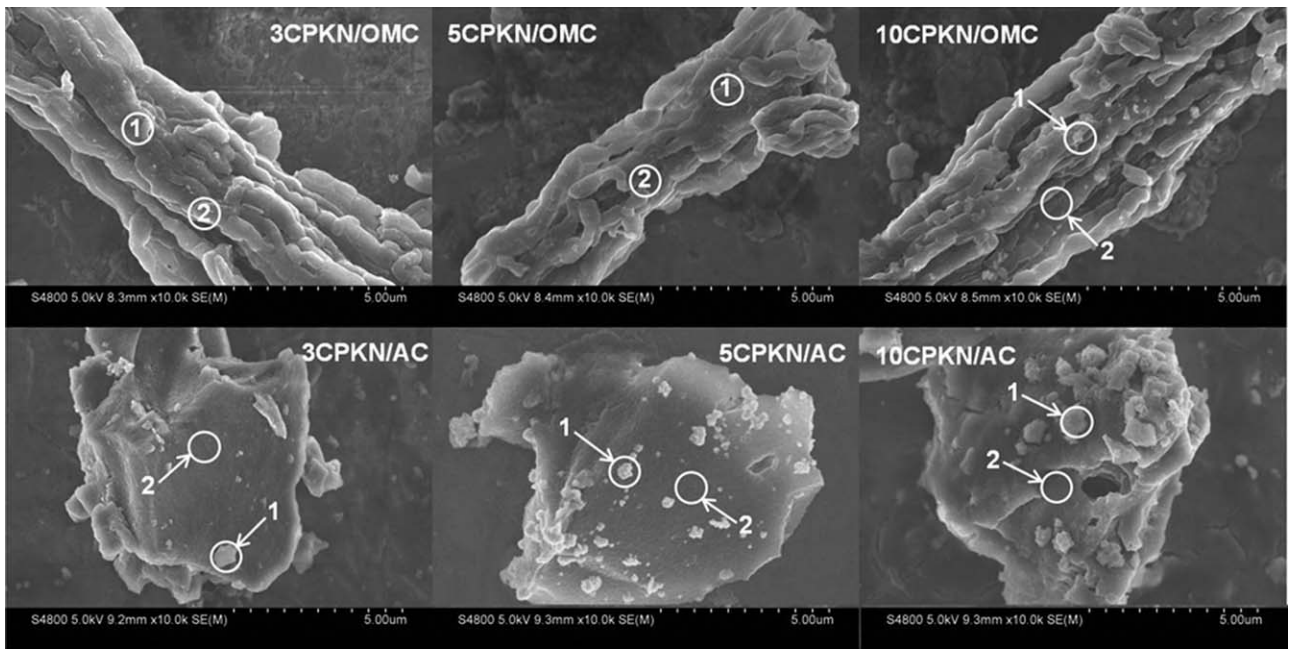

Figure 3. SEM images of nCPKN/OMC and nCPKN/AC.

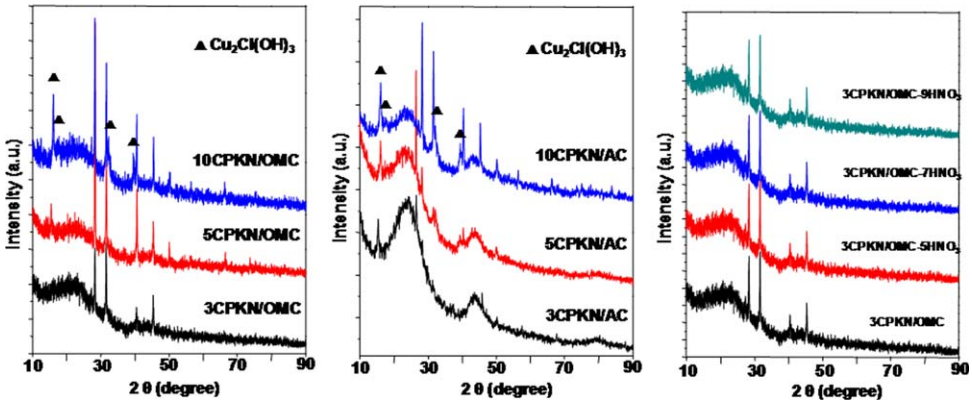

Figure 4. X-ray diffraction spectra for nCPKN/OMC, nCPKN/AC and 3CPKN/OMC-mHNO$_3$.

[Color figure can be viewed in the online issue, which is available at wileyonlinelibrary.com.]

The content of K and Na in area 1 is much higher than area 2, indicating incomplete dispersion of K and Na. However, some sodium and potassium was detected in regions where there are no large crystals, suggesting that these elements are dispersed throughout the catalyst. This phenomenon is in accordance with previous results reported by Bell and coworkers.[14] In order to clarify the structure of the active species in KCl-NaOH-$PdCl_2$-$CuCl_2$/AC catalyst, they used SEM to analyze the as-prepared catalyst. The results showed that some unsmooth regions were decorated with large crystallites made of KCl and NaCl. In our work, for low loading nCPKN/OMC catalysts, elements were evenly distributed (seen in Table 2), indicating that active components are highly dispersed. However, the active species have partly aggregated on the outside of the support channel pores only on high-loading samples (e.g., 10CPKN/OMC).

In order to compare the dispersion of active species on OMCs and AC, samples using AC as the support were also prepared with the loading ranged from 3 to 10%. Figure 3 shows SEM images of catalysts with different supports. We can observe that bright spots are distributed over the surface of catalysts with AC as the support, and the phenomenon of particle condensation becomes more serious when the catalyst loading increases, especially on 10CPKN/AC. While the surface of catalysts with OMC as the support is smooth and there are very small particles only on high-loading samples, e.g., 10CPKN/OMC. This is identical with the results of TEM. The elementary composition of areas with and without bright spots (areas 1 and 2 in Figure 3) were identified by EDX and results are shown in Table 2 (with regard to highly dispersed samples, 3CPKN/OMC and 5CPKN/OMC, the detection regions were chosen randomly). Cu, Cl, K and Na were well dispersed throughout the nCPKN/OMC catalysts. Until the loading increased to 10% Cu, the content of Cl, K and Na became heterogeneous. These results demonstrate that active components on OMCs disperse better than that on AC.

XRD spectra for catalysts nCPKN/OMC and nCPKN/AC are shown in Figure 4. All samples exhibit features for disordered graphite (very broad peaks at 23 and 44°).[33] It can be recognized that characteristic peaks for Cu species

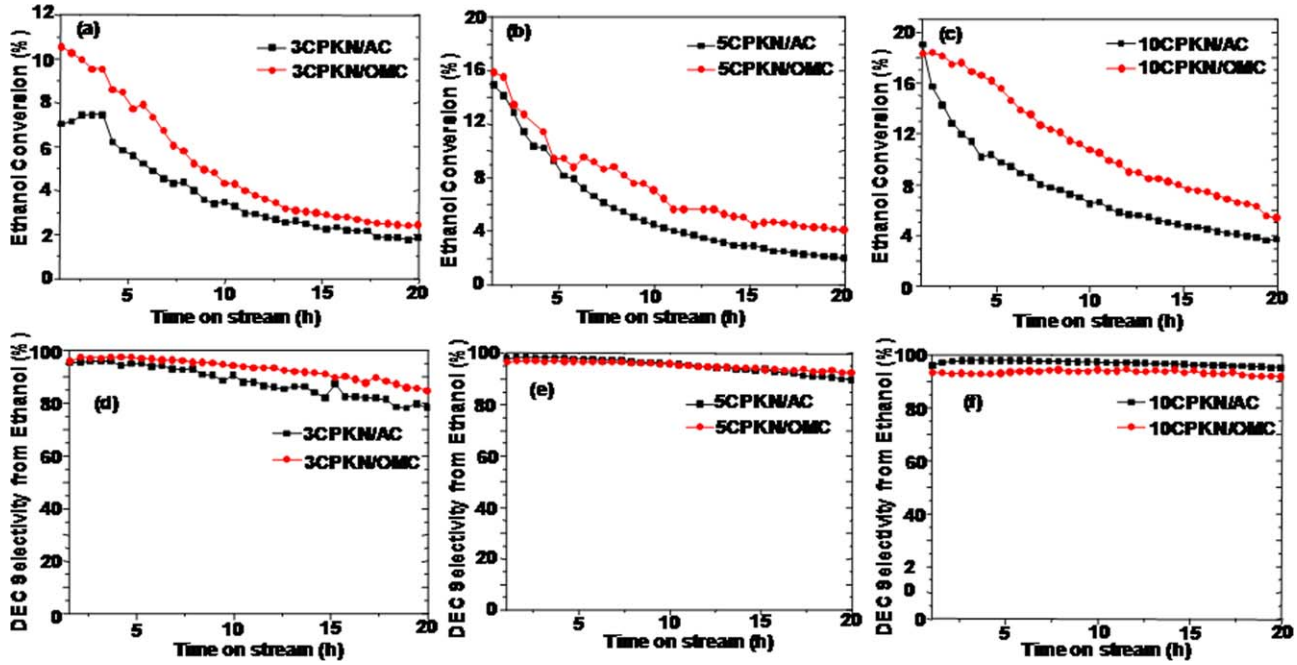

Figure 5. Catalytic properties for nCPKN/OMC and nCPKN/AC: (a-c) ethanol conversion, and (d-f) DEC selectivity.

[Color figure can be viewed in the online issue, which is available at wileyonlinelibrary.com.]

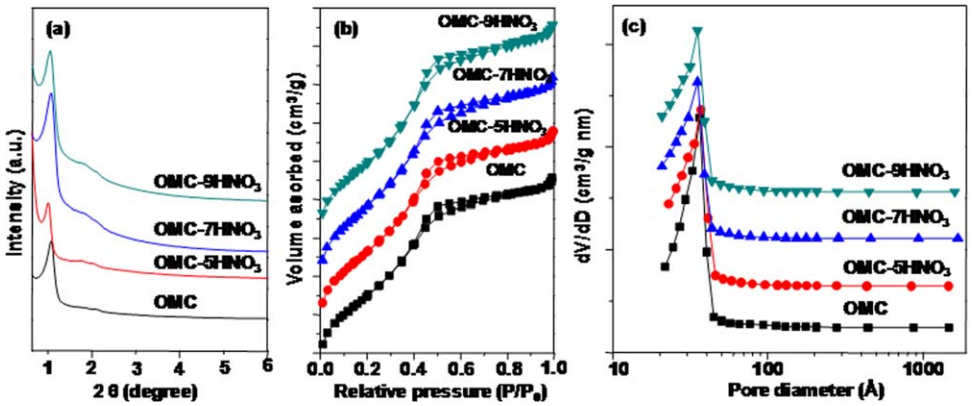

Figure 6. (a) Small-angle XRD patterns, (b) N_2 sorption isotherms, and (c) pore-size distributions of OMC before and after being treated by $mHNO_3$.

[Color figure can be viewed in the online issue, which is available at wileyonlinelibrary.com.]

Table 3. Textural Parameters of OMC Before and After Being Treated by $mHNO_3$

Support	BET area (m^2/g)	Micropre area (m^2/g)	Mesopore area (m^2/g)	Micropore volume (cm^3/g)	Mesopore volume (cm^3/g)	Total volume (cm^3/g)	Average pore diameter (Å)
OMC	1250.8	20.3	1230.4	0.02	1.22	1.24	35
OMC-5HNO_3	1228.3	43.2	1185.1	0.02	1.15	1.17	35
OMC-7HNO_3	1313.7	92.1	1221.7	0.04	1.04	1.07	33
OMC-9HNO_3	1367.0	89.7	1277.3	0.04	1.09	1.13	33

($Cu_2Cl(OH)_3$, JCPDS # 25-0269) are observed in catalysts with AC as the support even the loading is low. The peak became sharper when the loading was increased. However, these peaks can be observed only on high loadings when OMC was used as the support, such as 5CPKN/OMC and 10CPKN/OMC. No peaks standing for $Cu_2Cl(OH)_3$ appeared on catalyst 3CPKN/OMC means that the Cu species are highly dispersed.[14,34] Therefore, we can conclude that OMCs are more beneficial for the dispersion of active components than AC. When the loading of active species on OMC increased, the peaks appeared and corresponded to copper species (JCPDS # 25-0269). This confirms that catalysts with different supports have identical active species. There are no peaks for Pd species for all catalysts due to low loading of $PdCl_2$, which is agreed with previous results.[14] For all samples (nCPKN/OMC and nCPKN/AC) with Cu loadings ranging from 3 to 10%, characteristic peaks for KCl and NaCl were observed at 28.3°, 40.5°, 50.1°, and 31.6°, 45.3°, 56.3°, respectively, with peak intensity enhancing when the loading was improved.

The results mentioned previously demonstrate that OMCs are more effective for the dispersion of active components than AC. Our results are also well agreed with the previous studies that using OMCs as support can make the metal particles highly dispersed.[35–37] The ordered pore structure of OMCs with high-surface area and large-pore volume attribute to the enhanced dispersion of loaded species compared to activated carbon.

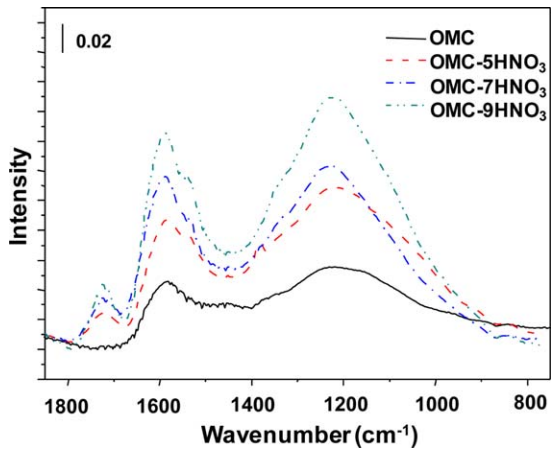

Figure 7. Transmission IR spectra of OMC before and after being treated by $mHNO_3$.

[Color figure can be viewed in the online issue, which is available at wileyonlinelibrary.com.]

Catalytic properties of nCPKN/OMC catalysts

Figure 5 illustrates the ethanol conversion and DEC selectivity from ethanol of catalysts with different supports. Notably, the 3CPKN/OMC catalyst with low loading and highly dispersed active species has higher initial catalytic activity than 3CPKN/AC. With the reaction preceded, this trend tended to mitigation, and ethanol conversion of 3CPKN/OMC maintained at 2.5%. It is a 26% improvement compared to 3CPKN/AC. The ethanol conversion used for comparison was chosen after 15-h reaction, at which time each

Table 4. Oxygen-Containing Group Content of Omc Before and After Being Treated by $mHNO_3$ Titrated by the Boehm Method

Support	Phenolic (mmole/g)	Lactonic (mmole/g)	Carboxylic acid (mmole/g)	Total acid groups (mmole/g)
OMC	0.60	0.30	0.02	0.92
OMC-5HNO_3	0.33	0.78	0.84	1.95
OMC-7HNO_3	0.51	1.09	0.73	2.33
OMC-9HNO_3	0.71	0.81	1.00	2.52

Table 5. Surface Composition of the Fresh and Used Catalysts after 20-hour Reaction Calculated by XPS Data

	Cl/at.%		Cu/at.%	
Before/After	Bef.	Aft.	Bef.	Aft.
3CPKN/OMC	2.6	0.5	0.5	0.4
3CPKN/OMC-5HNO_3	2.5	1.3	0.5	0.4
3CPKN/OMC-7HNO_3	2.8	1.6	0.4	0.4
3CPKN/OMC-9HNO_3	2.8	1.5	0.5	0.5

catalyst deactivated at a similar rate. When the loading of active components increased, the ethanol conversion was at the same level for two kinds of catalysts at beginning of the reaction. However, with the reaction proceeded, the enhanced performance of nCPKN/OMC was more obvious. Specially, for catalysts with loading of 5% Cu, the ethanol conversion has an enhancement of 65%. In addition, the ethanol conversion of 10CPKN/OMC has increased 64% compared to 10CPKN/AC. It can be concluded that catalysts using OMCs as support have better catalytic activity than catalysts using AC as support. Even though the catalysts deactivated with the reaction progressing, the DEC selectivity mainly remains unchanged (no more than 5% decline with 20-h reaction) for all nCPKN/OMC catalysts. However, the selectivity reaches up to above 95%. The explanations of deactivation have focused on the loss of chlorine that plays an important role in electron transfer during the reaction.[12,38–40] In order to explore the cause of deactivation of the catalysts, fresh and used (20-h test) samples were analyzed by XPS (Table 5). Upon the reaction, the content of active component, Cu, keeps stable, while the content of Cl has dropped from 2.6 to 0.5%. This means that the loss of chlorine cannot be eliminated from deactivation reasons, and the experiment result is consistent with previous work.

From the results of XRD (Figure 4), we can recognize that the active species are same in both kinds of catalysts. However, OMCs have better dispersibility than AC, which can be obtained from the results of TEM, SEM and XRD (Figures 2, 3, and 4). Thus, the catalytic activities of catalysts are strongly dependent on the dispersibility of the supports and the highly dispersed active species are helpful to improve the reaction activity of nCPKN/OMC catalysts.

Surface modification

For carbon material, the surface OCGs play an important role in anchoring the active species (e.g., preventing the loss

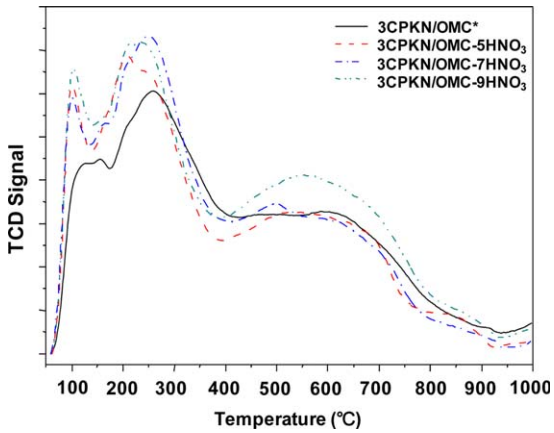

Figure 9. NH_3-TPD profiles of catalysts made from supports before and after being treated by $mHNO_3$.

[Color figure can be viewed in the online issue, which is available at wileyonlinelibrary.com.]

of chlorine species).[41–43] However, since most of OCGs (carboxylic) exhibited acidity, excessive OCGs were not favorable for oxidative carbonylation. This is because the target product DEC can decompose on the excessive acid center.[44,45] Thus, it is crucial to gain a certain level of oxide containing groups.[15] Therefore, OMCs were treated by HNO_3 to increase the oxide containing groups.[46–48]

For the sake of detecting whether the ordered structure of OMCs was maintained after being treated by HNO_3, the small-angle XRD patterns, N_2-sorption isotherms and pore size distributions of OMCs before and after being treated by $mHNO_3$ have been performed (Figure 6). It was obvious that the 2-D p6 mm hexagonal mesopore structure was preserved after HNO_3 oxidation, even the concentration of HNO_3 raised up to 9M. The definite textural parameters of OMCs were shown in Table 3, which confirms that the structure of OMCs was kept on HNO_3 treatment.

Surface groups on OMCs and OMC-$mHNO_3$ were characterized by transmission IR spectra and the Beohm titration. Characterization of OCGs before and after being treated by different concentrations of HNO_3 through IR is presented in Figure 7. Bands were observed in the regions of 1000–1400 cm^{-1}, which are attributed to characteristic of C—O stretching vibrations in ethers, phenols, esters, lactones, carboxylic acids, and carbonates and to O—H bending modes in phenols; a broad band at 1580 cm^{-1} is due to aromatic C=C

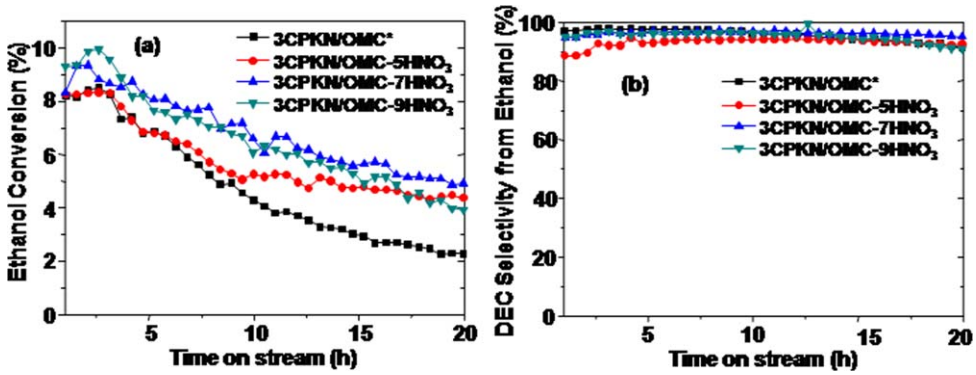

Figure 8. Catalytic properties of catalysts made from supports before and after being treated by $mHNO_3$: (a) ethanol conversion, and (b) DEC selectivity from ethanol.

[Color figure can be viewed in the online issue, which is available at wileyonlinelibrary.com.]

stretching vibrations; and bands observed in the region of 1660–1750 cm^{-1} are due to C═O stretching vibrations in carboxylic acids, lactones, and other C═O-containing groups.[15] After being treated by HNO_3, intensity of the bands in the regions of 1000–1400 cm^{-1} and 1660–1750 cm^{-1} increases, indicating that the treatment have improved OCGs on the OMCs surface. Intensity of these bands increases along with the incremental concentration of HNO_3.

Table 4 summarizes the Boehm titrate results for the OCGs content of OMCs before and after being treated by different concentration of HNO_3. After oxidation, the lactonic groups and carboxylic acid groups have a significant increase compared to untreated OMC. The total acid groups have increased in sequence when the concentration of HNO_3 increased, from 0.92 to 2.52 mmol/g, which is confirmed by IR spectra analyze results. These results show that the surface OCGs of OMCs have been regulated successfully under the condition that OMCs' ordered structure maintained.

Figure 8 presents the catalytic properties of catalysts before and after being treated by different concentration of HNO_3. These kinds of catalysts almost have the same catalytic activity at the beginning of reaction, but the stability of the catalysts is different. Compared to the catalyst using untreated support, deactivation trend of the catalyst slowed when using OMCs treated by HNO_3 as the support. This phenomenon becomes obvious along with the improved concentration of HNO_3. Also the decrease content of chlorine has been mitigated (Table 5). After reaction, chlorine content of catalyst 3CPKN/OMC has dropped from 2.6 to 0.5%, while the catalyst used OMC-mHNO_3 as support lessened slightly, from 2.8 to 1.5% approximately. The state of active species on treated OMCs was characterized by XRD, shown in Figure 4. No speaks regarding to copper species appear on catalysts 3CPKN/OMC-mHNO_3, indicating that active components are highly dispersed. This is same as the active species on untreated OMCs. The results of IR spectra and the Beohm titration indicated the OCGs of OMCs were improved after HNO_3 treatment. The elevated OCGs have enhanced the anchor ability of the support, which in turn increase the stability of the catalysts. However, for a higher HNO_3 concentration treatment, e.g., 9M, the catalyst catalytic activity has slightly dropped compare to 3CPKN/OMC-7HNO_3. This is because the catalyst using OMC-9HNO_3 as the support possesses excessive amount of acid center (seen in Figure 9) which can cause the decomposition of product DEC in reaction process.

Conclusions

We have drawn a relationship between catalytic properties and dispersity of catalysts. Structural properties of OMCs including high-surface area and large-pore volume facilitate the dispersion of active components, which in turn makes nCPKN/OMC show a good catalytic performance in DEC synthesis. Compared to nCPKN/AC catalysts, catalytic activities have been improved by as much as 65% when OMCs were used as support. Stability of catalyst activity was achieved by treating the support with a suitable concentration of HNO_3. Surface properties of OMCs are in connection with the catalytic stability of catalysts. However, the quantitative relationship between surface OCGs and anchor ability of OMCs was also discussed.

Acknowledgment

The financial support from the National Natural Science Foundation of China (NSFC) (Grant No. 20876112, 20936003, 20576093), Specialized Research Fund for the Doctoral Program of Higher Education (SRFDP) (Grant No. 20090032110021), and the Program of Introducing Talents of Discipline to Universities (B06006) are gratefully acknowledged.

Literature Cited

1. Pacheco MA, Marshall CL. Review of dimethyl carbonate (DMC) manufacture and its characteristics as a fuel additive. *Energ Fuel*. 1997;11:2–29.
2. Moumouzias G, Ritzoulis G, Siapkas D, Terzidis D. Comparative study of $LiBF_4$, $LiAsF_6$, $LiPF_6$, and $LiClO_4$ as electrolytes in propylene carbonate-diethyl carbonate solutions for Li/$LiMn_2O_4$ cells. *J Power Sources*. 2003;122:57–66.
3. Herstedt M, Stjerndahl M, Nyten A, Gustafsson T, Rensmo H, Siegbahn H, Ravet N, Armand M, Thomas JO, Edstrom K. Surface chemistry of carbon-treated $LiFePO_4$ particles for Li-ion battery cathodes studied by PES. *Electrochem Solid State Lett*. 2003;6:202–206.
4. Zhang PB, Huang SY, Wang SP, Ma XB. Effect of extra-framework silicon on the catalytic activity of Cu beta zeolite catalyst for synthesis of diethyl carbonate by oxidative carbonylation of ethanol. *Chem Eng J*. 2011;172:526–530.
5. Zhang PB, Ma XB. Catalytic synthesis of diethyl carbonate by oxidative carbonylation of ethanol over $PdCl_2$/Cu-HMS catalyst. *Chem Eng J*. 2010;163:93–97.
6. Zhang PB, Wang SP, Chen S, Zhang Z, Ma XB. The effects of promoters over $PdCl_2$-$CuCl_2$/HMS catalysts for the synthesis of diethyl carbonate by oxidative carbonylation of ethanol. *Chem Eng J*. 2008;143:220–224.
7. Xiong H, Mo WL, Hu JL, Bai RX, Li GX. CuCl/phen/NMI in homogeneous carbonylation for synthesis of diethyl carbonate: highly active catalyst and corrosion inhibitor. *Ind Eng Chem Res*. 2009;48:10845–10849.
8. Dunn BC, Guenneau C, Hilton SA, Pahnke J, Eyring EM, Dworzanski J, Meuzelaar HLC, Hu JZ, Solum MS, Pugmire RJ. Production of diethyl diethyl carbonate from ethanol and carbon monoxide over a heterogeneous catalyst. *Energ Fuel*. 2001;16:177–181.
9. Liu TC, Chang CS. Vapor-phase oxidative carbonylation of ethanol over CuCl═$PdCl_2$/C catalyst. *Appl Catal A*. 2006;304:72–77.
10. Roh NS, Dunn BC, Eyring EM, Pugmire RJ, Meuzelaar HLC. Production of diethyl carbonate from ethanol and carbon monoxide over a heterogeneous catalytic flow reactor. *Fuel Process Technol*. 2003;83:27–38.
11. Jiang XZ, Su YH, Lee BJ, Chien SH. A study on the synthesis of diethyl oxalate over Pd/α-Al_2O_3 catalysts. *Appl Catal A*. 2001;211:47–51.
12. Zhang Z, Ma XB, Zhang PB, Li YM, Wang SP. Effect of treatment temperature on the crystal structure of activated carbon supported $CuCl_2$-$PdCl_2$ catalysts in the oxidative carbonylation of ethanol to diethyl carbonate. *J Mol Catal A*. 2007;266:202–206.
13. Zhang Z, Ma XB, Zhang J, He F, Wang SP. Effect of crystal structure of copper species on the rate and selectivity in oxidative carbonylation of ethanol for diethyl carbonate synthesis. *J Mol Catal A*. 2005;227:141–146.
14. Briggs DN, Lawrence KH, Bell AT. An investigation of carbon-supported $CuCl_2$/$PdCl_2$ catalysts for diethyl carbonate synthesis. *Appl Catal A*. 2009;366:71–83.
15. Briggs DN, Bong G, Leong E, Oei K, Lestari G, Bell AT. Effects of support composition and pretreatment on the activity and selectivity of carbon-supported $PdCu_nCl_x$ catalysts for the synthesis of diethyl carbonate. *J Catal*. 2010;276:215–228.
16. Punnoose A, Seehra MS, Dunn BC, Eyring EM. Characterization of $CuCl_2$/$PdCl_2$/activated carbon catalysts for the synthesis of diethyl carbonate. *Energ Fuel*. 2001;16:182–188.
17. Yuan YZ, Cao W, Weng WZ. $CuCl_2$ immobilized on amino-functionalized MCM-41 and MCM-48 and their catalytic performance toward the vapor-phase oxy-carbonylation of methanol to dimethylcarbonate. *J Catal*. 2004;228:311–320.
18. Grzybek T, Pasel J, Papp H. Supported manganese catalysts for the selective catalytic reduction of nitrogen oxides with ammonia. *Phys Chem Chem Phys*. 1999;1:341–348.
19. Ryoo R, Joo SH, Kruk M, Jaroniec M. Ordered mesoporous carbons. *Adv Mater*. 2001;13:677–681.

20. Zhao XC, Wang AQ, Yan JW, Sun GQ, Sun LX, Zhang T. Synthesis and electrochemical performance of heteroatom-incorporated ordered mesoporous carbons. *Chem Mater.* 2010;22:5463–5473.
21. Foley HC. Carbogenic molecular sieves: synthesis, properties and applications. *Microporous Mater.* 1995;4:407–433.
22. Zhuang X, Wan Y, Feng CM, Shen Y, Zhao DY. Highly efficient adsorption of bulky dye molecules in wastewater on ordered mesoporous carbons. *Chem Mater.* 2009;21:706–716.
23. Wang JC, Xiang CS, Liu Q, Pan YB, Guo JK. Ordered mesoporous carbon/fused silica composites. *Adv Funct Mater.* 2008;18:2995–3002.
24. He C, Hu XJ. Anionic dye adsorption on chemically modified ordered mesoporous carbons. *Ind Eng Chem Res.* 2011;50:14070–14083.
25. Zhang JY, Deng YH, Wei J, Sun ZK, Gu D, Bongard H, Liu C, Wu HH, Tu B, Schuth F, Zhao DY. Design of amphiphilic ABC triblock copolymer for templating synthesis of large-pore ordered mesoporous carbons with tunable pore wall thickness. *Chem Mater.* 2009;21:3996–4005.
26. Jun S, Joo SH, Ryoo R, Kruk M, Jaroniec M, Liu Z, Ohsuna T, Terasaki O. Synthesis of new, nanoporous carbon with hexagonally ordered mesostructure. *J Am Chem Soc.* 2000;122:10712–10713.
27. Zeng J, Francia C, Dumitrescu MA, Monteverde Videla AHA, Ijeri VS, Specchia S, Spinelli P. Electrochemical performance of Pt-based catalysts supported on different ordered mesoporous carbons (Pt/OMCs) for oxygen reduction reaction. *Ind Eng Chem Res.* 2011:51:7500–7509.
28. Choi M, Heo W, Kleitz F, Ryoo R. Facile synthesis of high quality mesoporous SBA-15 with enhanced control of the porous network connectivity and wall thickness. *Chem Commun.* 2003; 0:340–1341.
29. Salame II, Bandosz TJ. Comparison of the surface features of two wood-based activated carbons. *Ind Eng Chem Res.* 2000;39:301–306.
30. Kilduff JE, King CJ. Effect of carbon adsorbent surface properties on the uptake and solvent regeneration of phenol. *Ind Eng Chem Res.* 1997;36:1603–1613.
31. Bashkova S, Bagreev A, Bandosz TJ. Effect of surface characteristics on adsorption of methyl mercaptan on activated carbons. *Ind Eng Chem Res.* 2002;41:4346–4352.
32. Boehm HP. Some aspects of the surface chemistry of carbon blacks and other carbons. *Carbon.* 1994;32:759–769.
33. Manivannan A, Chirila M, Giles NC, Seehra MS. Microstructure, dangling bonds and impurities in activated carbons. *Carbon.* 1999;37:1741–1747.
34. Xiao FS, Zheng S, Sun J, Yu R, Qiu S, Xu R. Dispersion of inorganic salts into zeolites and their pore modification. *J Catal.* 1998;176:474–487.
35. Liu SH, Lu RF, Huang SJ, Lo AY, Chien SH, Liu SB. Controlled synthesis of highly dispersed platinum nanoparticles in ordered mesoporous carbons. *Chem Commun.* 2006;0:3435–3437.
36. Lu AH, Li WC, Hou Z, Schuth F. Molecular level dispersed Pd clusters in the carbon walls of ordered mesoporous carbon as a highly selective alcohol oxidation catalyst. *Chem Commun.* 2007;0:1038–1040.
37. Ryoo R, Joo SH, Choi SJ. Ordered mesoporous carbons exhibiting extraordinary metal dispersion. *Abstr Pap Am Chem Soc.* 2001;221:46.
38. Jiang R, Wang Y, Zhao X, Wang S, Jin C, Zhang C. Characterization of catalyst in the synthesis of dimethyl carbonate by gas-phase oxidative carbonylation of methanol. *J Mol Catal A.* 2002;185:159–166.
39. Ruixia J, Shufang W, Xinqiang Z, Yanji W, Chengfang Z. The effects of promoters on catalytic properties and deactivation-regeneration of the catalyst in the synthesis of dimethyl carbonate. *Appl Catal A.* 2003;238:131–139.
40. Curnutt GL. Catalytic vapor phase process for producieng dihydrocarbyl carbonates. US Patent 5,004,827. April 2, 1991.
41. Rodríguez-reinoso F. The role of carbon materials in heterogeneous catalysis. *Carbon.* 1998;36:159–175.
42. Wang XM, Li N, Webb JA, Pfefferle LD, Haller GL. Effect of surface oxygen containing groups on the catalytic activity of multi-walled carbon nanotube supported Pt catalyst. *Appl Catal B.* 2010;101:21–30.
43. Ros TG. Van Dillen AJ, Geus JW, Koningsberger DC. Surface oxidation of carbon nanofibres. *Chem Eur J.* 2002;8:1151–1162.
44. Plomp AJ, Su DS, Jong KPd, Bitter JH. On the nature of oxygen-containing surface groups on carbon nanofibers and their role for platinum deposition-an XPS and titration study. *J Phys Chem C.* 2009;113:9865–9869.
45. Anderson SA, Manthata S, Root TW. The decomposition of dimethyl carbonate over copper zeolite catalysts. *Appl Catal A.* 2005;280:117–124.
46. Park ED, Lee JS. Effect of surface treatment of the support on CO oxidation over carbon-supported wacker-type catalysts. *J Catal.* 2000;193:5–15.
47. Liu SX, Wang R. Modified activated carbon with an enhanced nitrobenzene adsorption capacity. *J Porous Mater.* 2011;18:99–106.
48. Tangsathitkulchai C, Ngernyen Y, Tangsathitkulchai M. Surface modification and adsorption of eucalyptus wood-based activated carbons: Effects of oxidation treatment, carbon porous structure and activation method. *Korean J Chem Eng.* 2009;26:1341–1352.

Manuscript received Aug. 10, 2012, and revision received Jan. 31, 2013.